J Mater Sci (2008) 43:1836–1843
DOI 10.1007/s10853-007-2375-2

Texture and microstructural development in gelcast barium hexaferrite

D. B. Hovis · K. T. Faber · E. A. Kenik

Received: 1 August 2007 / Accepted: 3 December 2007 / Published online: 18 January 2008

Abstract The development of texture in barium hexaferrite by templated grain growth was studied as a function of the $Fe_2O_3/BaCO_3$ ratio, B_2O_3 additions in the starting materials, and sintering temperature. A magnetic field was used to orient the template particles during the gelcasting process. Excess $BaCO_3$ resulted in abnormal grain growth and maximized texture, while B_2O_3 additions promoted coarsening, but no abnormal grain growth.

Introduction

Templated grain growth (TGG) is an effective method to induce crystallographic and morphological textures in highly anisotropic ceramics [1–6]. In this technique, a fine-grained, isotropic matrix is sintered with a small fraction of large, morphologically anisotropic "template" particles which are aligned during forming. During firing, only template grains and matrix grains with the same orientation as template grains are able to grow. Large template particles grow at the expense of small, misaligned matrix grains, resulting in a dense, highly textured microstructure.

D. B. Hovis · K. T. Faber (✉)
Department of Materials Science and Engineering, Robert R. McCormick School of Engineering and Applied Science, Northwestern University, Evanston, IL 60208-3108, USA
e-mail: k-faber@northwestern.edu

E. A. Kenik
Materials Science and Technology Division, Oak Ridge National Laboratory, Oak Ridge, TN, USA

Present Address:
D. B. Hovis
Department of Materials Science and Engineering, Case Western Reserve University, Cleveland, OH, USA

One disadvantage of most methods used for aligning the template particles for TGG is that the texture direction is tightly coupled to the sample geometry. Processing techniques like tape casting [3] and uniaxial pressing [1, 2] will cause morphologically anisotropic template particles to align due to shear forces, and as a result, the texture direction will always be directly related to the sample geometry.

Magnetic field-assisted gelcasting techniques afford significant texture in ceramics, such as Fe_2TiO_5, and offer a means to decouple texture from geometry [7–9]. Here, magnetically anisotropic powders, suspended in a solution containing organic monomers, are cast into the desired shape and polymerized to form a gelled body. The crystallographic texture is sustained through drying, polymer binder burnout, and sintering. Magnetic field-assisted gelcasting has been extended to TGG systems where template particles are magnetically anisotropic. This has been demonstrated by gelcasting templates of barium hexaferrite ($BaFe_{12}O_{19}$), a hexagonal ferrimagnetic ceramic, along with $BaCO_3$ with Fe_2O_3, in the presence of a magnetic field [5]. The use of a magnetic field to induce template alignment is appealing, as it allows the texture direction to be completely independent of sample geometry.

The processing of $BaFe_{12}O_{19}$, predominantly for permanent magnet applications, has received considerable attention over the years, particularly when produced via a reaction of $BaCO_3$ with Fe_2O_3 [10–12]. Both stoichiometry [10] and second phase additions (e.g. B_2O_3 or SiO_2) [13, 14] play critical roles in reaction control, sinterability, and grain growth in $BaFe_{12}O_{19}$. In the current paper, the importance of both stoichiometry and chemistry through additions of B_2O_3 on the microstructural development in templated $BaFe_{12}O_{19}$ is demonstrated.

Experimental procedure

The basic procedure for gelcasting in the $BaFe_{12}O_{19}$ system is discussed in detail in a previous paper [5]. Briefly, a mixture of iron (III) oxide, Fe_2O_3 (All-Chemie, Mt Pleasant, SC); barium carbonate, $BaCO_3$ (Alfa Aesar, St. Louis, MO); $BaFe_{12}O_{19}$ (Alfa Aesar); and, in some mixtures, B_2O_3 as boric acid (Alfa Aesar), was dispersed in an aqueous solution of *n*,*n*,*n*′,*n*-hydroxymethylacrylamide (Sigma–Aldrich Corp, St. Louis, MO) using Surfynol CT-131 (Air Products, Allentown, PA) as a dispersant. Particle sizes for Fe_2O_3 and $BaCO_3$ averaged less than 100 nm and 1 μm, respectively. The $BaFe_{12}O_{19}$ templates have a plate-shaped morphology with a major axis of 1–5 μm and an aspect ratio of ~10:1. The volume fraction of ceramic was 0.40. This mixture was vibratory milled with MgO-stabilized zirconia milling media (Zircoa Inc., Solon, OH) for 2 h to form a slurry. Polymerization was initiated with a 10 wt% ammonium persulfate solution (APS) (Alfa Aesar) and tetraethylmethylenediamine (TEMED) (Sigma–Aldrich) and cast into a suitable mold.

Molds were made from two 75 × 50 × 1 mm^3 glass slides separated by a neoprene gasket. Each glass slide was wrapped with Escal™ film (Mitsubishi Gas Chemical, New York, NY). The Escal™ sheet is a transparent multilayer polymer film with a vapor-deposited ceramic layer. The ceramic layer in the Escal™ film serves as both an oxygen and water barrier. The Escal™ film prevents oxygen from entering the slurry, since oxygen disrupts the polymerization process [15], inhibits premature drying, and provides an easy release from the final gel with no residue. The neoprene gasket was affixed to one Escal™-wrapped slide with fiberglass-reinforced double-sided tape, and the initiated slurry was poured into the mold. The other glass slide was then carefully lowered onto the top of the mold, taking care to expel any bubbles, which would disrupt the gel formation process. Plastic clips were used to keep the mold closed during gel formation.

The mold was placed between two 15 × 10 × 2 cm^3 plate magnets with a remnant field of 400–600 Gauss (0.04–0.06 T) in an oven at 40 °C for 45 min. The magnetic field aligned the $BaFe_{12}O_{19}$ template particles while the gel formed. Once removed from the oven and allowed to cool to room temperature, the gels were removed from their molds and sectioned parallel to the field direction to allow sintering at different temperatures.

The gels were allowed to dry at room temperature for 1 week before the polymer was burned out in a vented resistance-heated furnace. The furnace was heated at 1 °C/min to 600 °C with a 1-h hold. The samples were then transferred to a different resistance furnace for sintering. The heating and cooling rates of 10 °C/min were used in all cases with a 2-h hold at the sintering temperature.

In order to assess the densification and grain growth behavior, a full factorial design of experiments was performed. Three factors were considered: $Fe_2O_3/BaCO_3$ ratio, B_2O_3 content, and sintering temperature, giving a total of 12 trials. The $Fe_2O_3/BaCO_3$ ratio was tested at 6.0 (stoichiometric) and 5.6 (excess $BaCO_3$ and designated non-stoichiometric). The B_2O_3 content was tested at 0% or 1% by mole. Sintering was accomplished at one of the three temperatures, 1235, 1280, or 1325 °C, as determined from a furnace calibration with an uncertainty of ±5 °C. Density was measured by the Archimedes method [16].

The texture in samples of at least 85% of theoretical density was measured using Orientation Imaging Microscopy (OIM) [17, 18] mapping on a Philips XL30 SEM with a TSL electron backscattered diffraction detector. The samples were inclined to 70° with respect to the electron beam. A pole figure map was generated, and the peak texture was measured. The texture measurement used was the maximum multiples of a random distribution (MRD) [19]. The maximum MRD measurement compares the probability that a grain has a particular orientation to the same probability for a random distribution. An MRD of one indicates a random distribution, whereas an MRD greater than one indicates that a given grain is more likely to be oriented in the texture direction.

Results

Density

The density of samples of the various compositions as a function of sintering temperature is shown in Fig. 1. It is clear that both B_2O_3 and additional $BaCO_3$ independently enhance the densification of $BaFe_{12}O_{19}$ at lower temperatures. The non-stoichiometric sample with excess $BaCO_3$ in combination with B_2O_3 produces greater densification

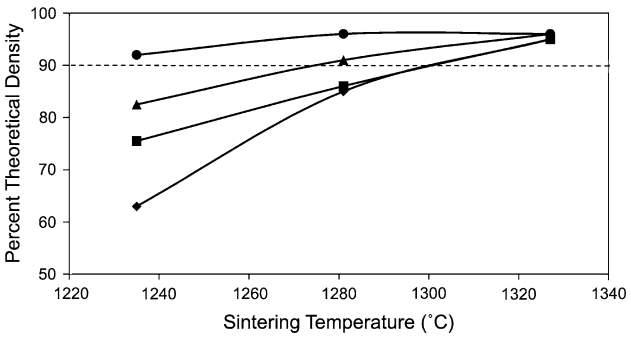

Fig. 1 Density of $BaFe_{12}O_{19}$ prepared as stoichiometric (◆), stoichiometric with B_2O_3 (■), non-stoichiometric (▲), and non-stoichiometric with B_2O_3 (●) as a function of sintering temperature. The dotted line indicates the density above which templated grain growth generally occurs, according to Ref. [20]

still, with the peak density reaching 1280 °C. At 1325 °C, there is very little difference between the densities of the four compositions, although the stoichiometric samples without B_2O_3 developed roughened surfaces upon firing at this temperature.

Microstructure

While the densities resulting from firing at 1325 °C are similar among the different compositions, the microstructures develop via different paths and show significantly different character. The stoichiometric samples at 1280 °C (Fig. 2a) show aligned templates and very little grain growth (very low density). At 1325 °C (Fig. 2b, c), the templates have either grown to consume most of the matrix or the matrix grains demonstrated anisotropic grain growth and adopted the orientation and habit of the templates. The stoichiometric samples containing B_2O_3 at 1280 °C (Fig. 3a) show little or no template growth. At 1325 °C (Fig. 3b), moderate grain growth is seen, but visually the grain alignment does not appear to be as strong as in other samples at this temperature.

The non-stoichiometric samples show more abnormal grain growth at 1280 °C (Fig. 4a) than either of the stoichiometric types, which is to be expected based on the higher densities of the non-stoichiometric samples. For these samples, it is clear that only a few templates grow, and many of them are quite large, even at 1280 °C. At 1325 °C (Fig. 4b), these samples exhibit considerable grain growth, with major axes for some grains in excess of 1 mm. Finally, the non-stoichiometric samples containing B_2O_3 show significant template growth, even at 1235 °C (Fig. 5a); however, the average aspect ratio is less than the non-stoichiometric samples prepared with no B_2O_3. At 1280 °C (Fig. 5b), the templates appear to have consumed all the matrix grains. No further grain growth appears to occur in the samples sintered at 1325 °C (Fig. 5c).

Both non-stoichiometric samples (with and without B_2O_3) also show the appearance of barium-rich second phases. In the case of samples with only excess $BaCO_3$, this second phase is believed to be a small amount of barium monoferrite, $BaFeO_4$, which is only apparent when imaged with backscattered electrons (Fig. 6a). Energy dispersive spectroscopy (EDS) mapping (Fig. 6b, c) shows that this phase is barium rich and iron depleted with respect to the matrix. Samples with B_2O_3 also contain a barium-rich phase, which diffuses to the sample surface during thermal etching. This phase is optically transparent (Fig. 7), with no observable grain boundaries and no detectable peaks in X-ray diffraction (XRD). EDS analysis also shows that this phase is rich in barium with very low iron content.

Texture

An OIM measurement is shown in Fig. 8 for a non-stoichiometric sample with no B_2O_3 and fired at 1325 °C. The SEM image is shown in Fig. 8a with the corresponding OIM grain map in Fig. 8b, where regions of identical color represent like crystallographic orientations, and the resultant pole figure is given in Fig. 8c. This sample had the strongest fiber texture of all the samples, with a maximum MRD of 63. The maximum MRD value for each sample is provided in Table 1. All samples demonstrate some texture, compared to a non-magnetically aligned control sample studied earlier [5]. In general, greater texture is achieved with higher sintering temperatures. It should be

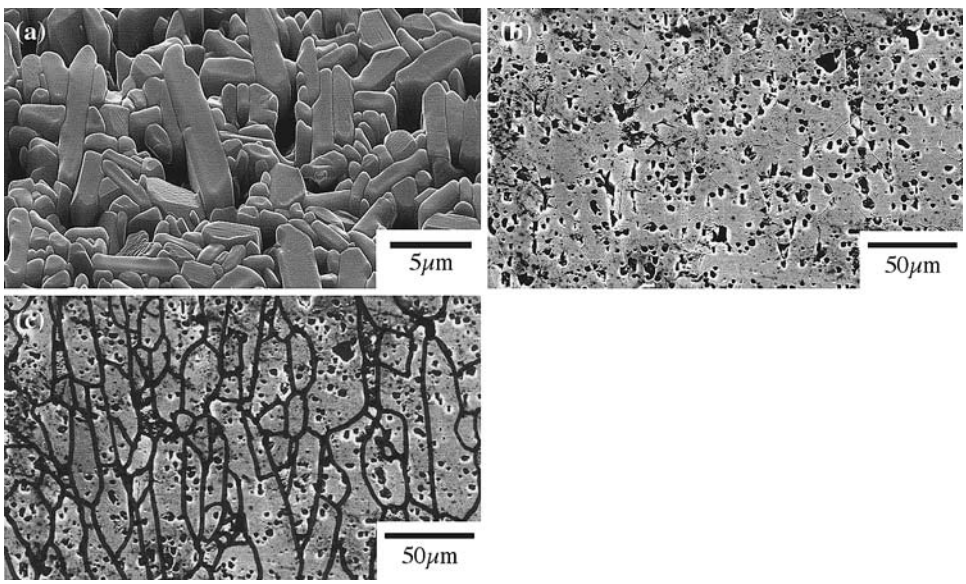

Fig. 2 SEM micrographs of stoichiometric $BaFe_{12}O_{19}$ samples sintered at (**a**) 1280 °C (**b**) 1325 °C (**c**) same as (**b**), but with the grain boundaries highlighted

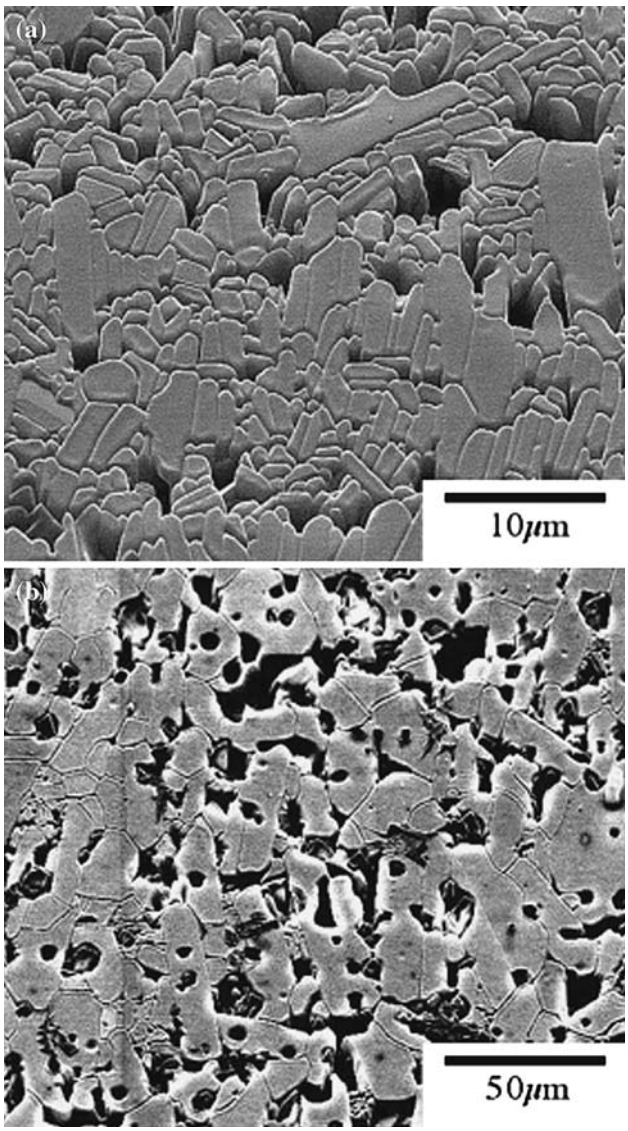

Fig. 3 SEM micrographs of stoichiometric $BaFe_{12}O_{19}$ samples containing B_2O_3 sintered at (**a**) 1280 °C and (**b**) 1325 °C, showing significant grain pullout

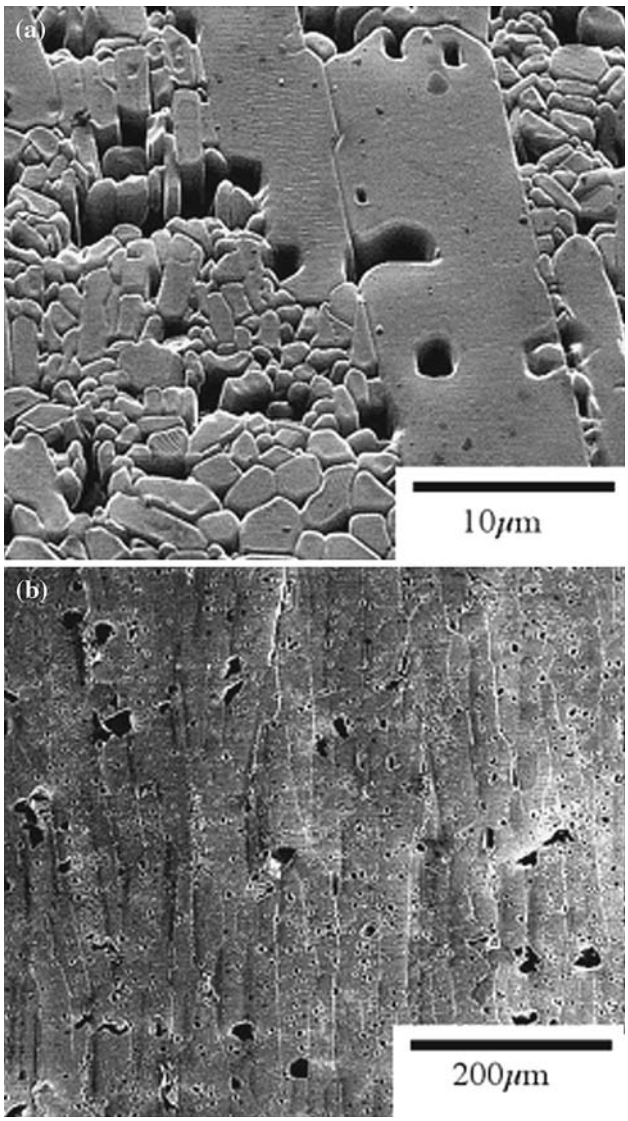

Fig. 4 SEM micrographs of the non-stoichiometric $BaFe_{12}O_{19}$ samples sintered at (**a**) 1280 °C and (**b**) 1325 °C

noted that these measurements should be considered semi-quantitative at best and are mainly useful for comparing differing degrees of texture between similar samples. Further interpretation of these measurements is provided in the discussion.

Discussion

The previous observation that significant template growth begins when the density reaches 90% of theoretical is consistent with the systems studied here [20]. Little to no template growth appears to occur in the samples below 90% of theoretical density, as shown in Figs. 2a and 3a. The non-stoichiometric samples sintered at 1280 °C had a density close to 90% of theoretical and provide a good example of the onset of abnormal grain growth (Fig. 4a).

The effect of composition on the final microstructure of the various samples shows no specific trends, but can be understood largely on the basis of the $Fe_2O_3/BaCO_3$ ratio. It has been demonstrated that an excess of $BaCO_3$ (ratio < 6) promotes abnormal grain growth, whereas samples with excess Fe_2O_3 (ratio > 6) require higher sintering temperatures to achieve equivalent densities [10, 11]. Such evidence explains the behavior of the non-stoichiometric samples ($Fe_2O_3/BaCO_3 = 5.6$), where the excess $BaCO_3$ promotes densification and abnormal grain growth (Fig. 4). Steier et al. have explained this observation by the formation of a second phase of barium monoferrite ($BaFeO_4$) [12]. This second phase impedes the

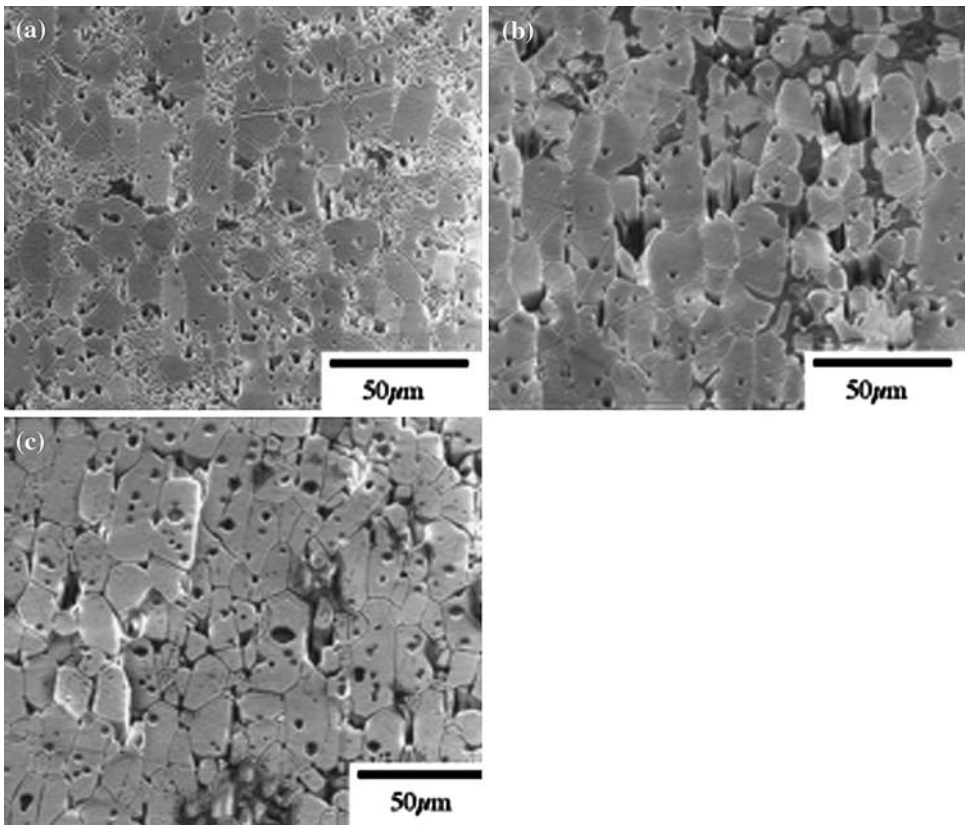

Fig. 5 SEM micrographs of the non-stoichiometric $BaFe_{12}O_{19}$ samples containing B_2O_3sintered at (**a**) 1235 °C, (**b**) 1280 °C, and (**c**) 1325 °C

growth of all but the largest of grains, leading to abnormal grain growth [21]. The monoferrite phase is known to form a eutectic with hexaferrite at temperatures above 1315 °C [10, 22–24]. Hence, the molten phase seen in Fig. 5 likely enhances grain growth through solution-reprecipitation.

The behavior of the stoichiometric samples can also be understood on the basis of the $Fe_2O_3/BaCO_3$ ratio and the required mass transport to stoichiometrically homogenize the sample, which is necessary for densification in $BaFe_{12}O_{19}$. As a co-precipitated precursor was not used, it is hypothesized that slight composition fluctuations are present (of the order of the starting particle size), such that some regions in the sample have excess $BaCO_3$ and some regions have excess Fe_2O_3 [12, 25]. The regions with excess $BaCO_3$ will densify and undergo grain growth before the regions with excess Fe_2O_3. As the sintering temperature is increased to 1325 °C, it is anticipated that some localized regions with higher barium will be liquid, again due to the monoferrite–hexaferrite eutectic [10, 22–24]. This non-homogeneous densification leads to the previously mentioned distortion, but also accounts for the surprising amount of grain growth in many of these samples.

The stoichiometric samples containing B_2O_3 exhibited the least grain growth and the least texture at 1325 °C. The most likely explanation for this behavior is the presence of the low melting point B_2O_3 (m.p. = 450 °C). As before, homogenization is required before densification, and the B_2O_3 forms a liquid which speeds homogenization of the compact before densification and grain growth. This liquid forms at a much lower temperature than in the stoichiometric composition without B_2O_3. The dominant grain growth mechanism is likely coarsening rather than abnormal grain growth. The template grains are not significantly favored over matrix grains, leading to much less texture than in all other compositions used here. One puzzling result is the lower texture measurement for these samples sintered at 1325 °C than those sintered at 1280 °C. This was most likely a case of sampling bias during the OIM measurements. OIM works best on dense regions of the sample. For the samples sintered at 1280 °C, the densest regions contained stacks of templates, skewing the result, while samples sintered at 1325 °C show significant grain pullout.

For non-stoichiometric samples containing B_2O_3, densification and template grain growth occur at lower temperatures than in all the other compositions. Once maximum density has been achieved and the templates have grown together, little further grain growth is observed. In addition, a second, barium-rich glass phase (Fig. 7) forms during densification. If we consider the excess $BaCO_3$ and B_2O_3 present in these samples, the

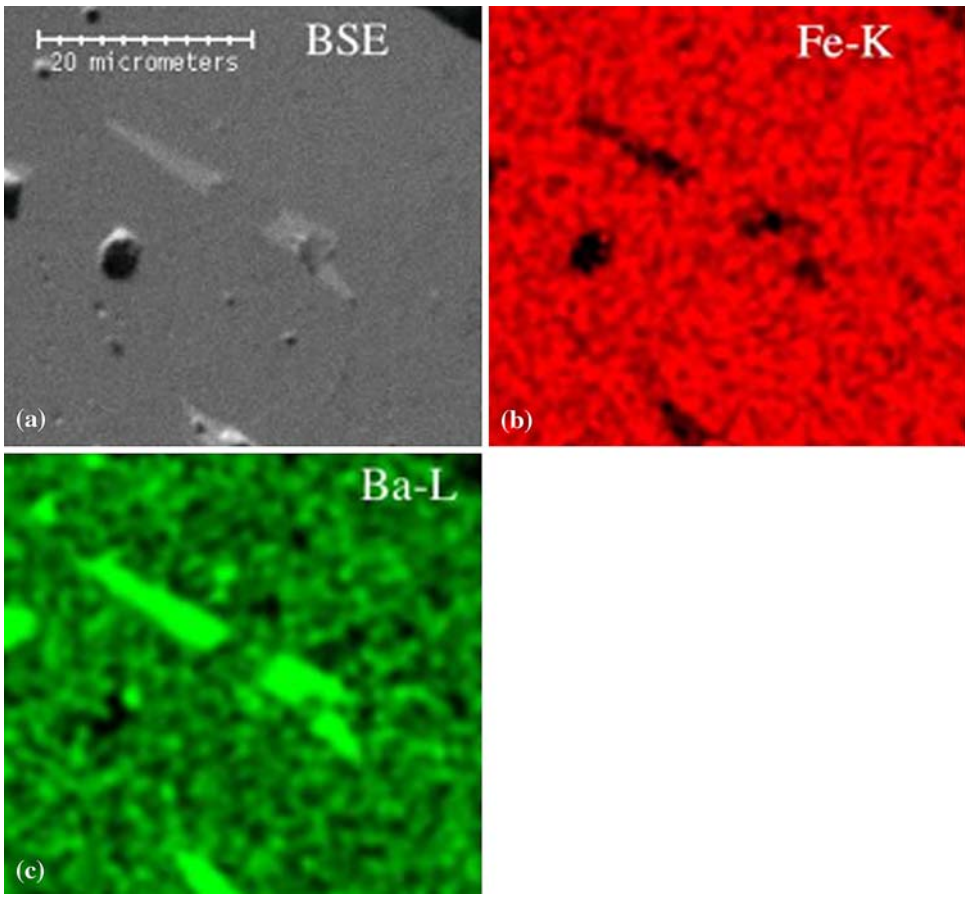

Fig. 6 (**a**) Backscattered SEM image showing a second phase (lighter region) in a non-stoichiometric $BaFe_{12}O_{19}$ sample. (**b**) An EDS map of the Fe K-line, showing depleted iron content in this phase. (**c**) An EDS map of the Ba L-line, showing higher barium content in this phase than in the surrounding matrix

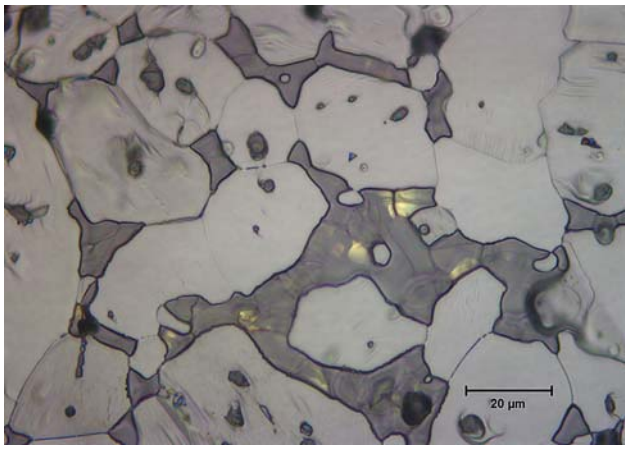

Fig. 7 An optical micrograph of a non-stoichiometric $BaFe_{12}O_{19}$ sample containing B_2O_3, etched at 1125 °C for 2 h to bring additional darker phase to the surface. This phase is barium rich and optically transparent. The grain boundaries which seem to be in the darker phase are actually from grains underneath, which was confirmed by varying the focal depth

composition is approximately 20% B_2O_3–80% $BaCO_3$ by weight. The BaO–B_2O_3 phase diagram shows a eutectic in the vicinity of this composition, with a melting point of 915 °C [26]. In fact, barium borate fluxes have been used for the growth of single crystals of $BaFe_{12}O_{19}$ [27]. Thus, the development of the microstructure in the non-stoichiometric samples containing B_2O_3 is flux driven.

Conclusions

In the present study of templated grain growth of gelcast $BaFe_{12}O_{19}$, densification and grain growth is controlled by both the $Fe_2O_3/BaCO_3$ ratio and B_2O_3 additives. The four compositions studied here exhibited four different microstructural development mechanisms. Stoichiometric sample densification was dependent on local compositional inhomogeneities. Stoichiometric samples with B_2O_3 homogenized at lower temperatures and exhibited grain coarsening, rather than undergoing abnormal grain growth. With the addition of excess $BaCO_3$ and no B_2O_3, the samples underwent significant abnormal grain growth. Finally, the non-stoichiometric samples with B_2O_3 formed a barium borate glass phase which served as a flux for the growth of $BaFe_{12}O_{19}$.

The grain size and degree of texture in $BaFe_{12}O_{19}$ are strongly dependent on chemistry and firing temperature. A variety of microstructures in $BaFe_{12}O_{19}$ can be achieved by appropriate control of the processing parameters. Grain growth can be suppressed by using a stoichiometric

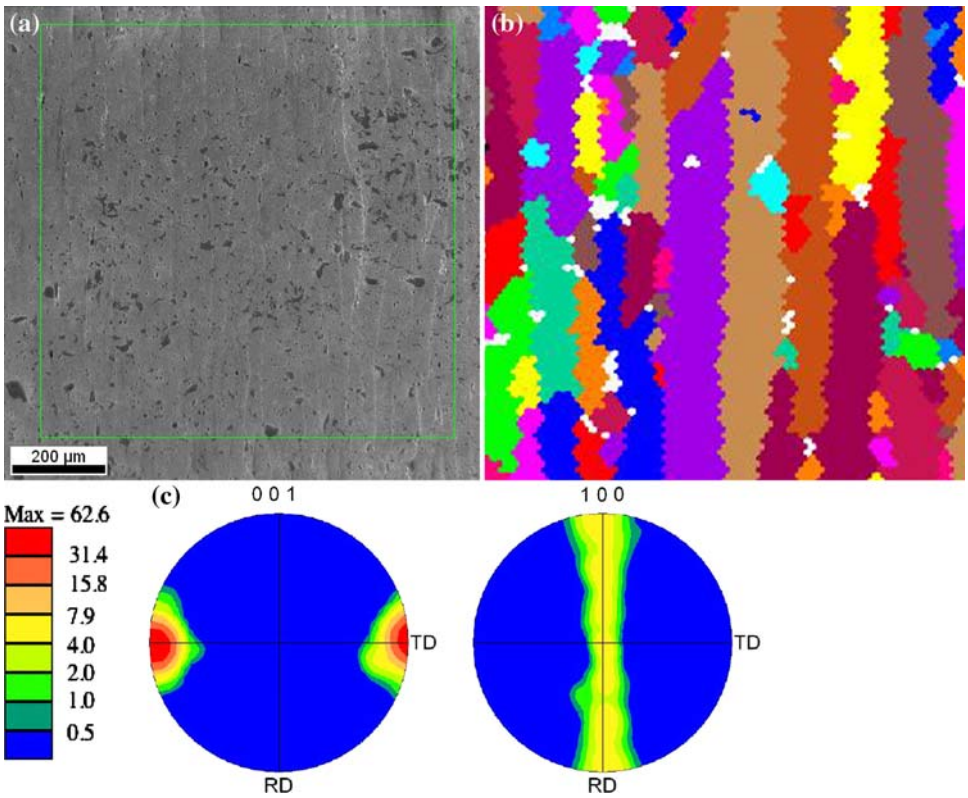

Fig. 8 An example of OIM measurement on a non-stoichiometric $BaFe_{12}O_{19}$ sample sintered at 1325 °C. (**a**) An SEM image of the region being mapped. (**b**) A unique grain map for this region (as determined by the OIM software) (**c**) Pole figures for the (001) and (100) crystallographic directions, showing strong fiber texture

Table 1 Texture measurements, reported as maximum of multiples of random distribution (MRD) for each sintering temperature and composition studied

Composition	Temperature (°C)	%Theoretical density	Maximum MRD
Stoichiometric	1280	85	10.7
	1325	96	34.4
Stoichiometric with B_2O_3	1280	86	23.9
	1325	95	14.5
Non-stoichiometric	1280	91	36.8
	1325	96	63.0
Non-stoichiometric with B_2O_3	1235	92	34.3
	1280	96	43.0
	1325	96	39.8

composition and an additive to enhance chemical homogenization. Alternatively, abnormal grain growth can be encouraged through non-stoichiometric chemistry and higher sintering temperatures. Using magnetic field-assisted gelcasting coupled with the appropriate chemistry, it is possible to control the abnormal grain growth to provide a dense, highly textured microstructure in $BaFe_{12}O_{19}$.

Acknowledgements This work was supported by the National Science Foundation under Grant Nos. DMR-9800257 and DMR-0520513. A portion of the electron microscopy was conducted in the SHaRE User Facility at the Oak Ridge National Laboratory, which is sponsored by the Division of Scientific User Facilities, Office of Science, U.S. Department of Energy.

References

1. Seabaugh MM, Kerscht IH, Messing GL (1997) J Am Ceram Soc 80:1181
2. Suvaci E, Seabaugh MM, Messing GL (1999) J Eur Ceram Soc 19:2465
3. Duran C, Trolier-McKinstry S, Messing GL (2000) J Am Ceram Soc 83:2203
4. Gonenli IE, Messing GL (2001) J Eur Ceram Soc 21:2495
5. Hovis DB, Faber KT (2001) Scripta Mater 44:2525
6. Messing GL, Sabolsky EM, Kwon S, Trolier-McKinstry S (2002) Key Eng Mater 206–2:1293
7. Paulik SW, Faber KT, Fuller ER Jr (1994) J Am Ceram Soc 77:454
8. Zimmerman MH, Faber KT, Fuller ER Jr (1997) J Am Ceram Soc 80:2725
9. Zimmerman MH, Baskin DM, Faber KT, Fuller ER Jr, Allen AJ, Keane DT (2001) Acta Mater 49:3231
10. Lacour C, Paulus M (1975) Physica Status Solidi A Appl Res 27:441
11. Lacour C, Paulus M (1975) Physica Status Solidi A Appl Res 28:71
12. Steier HP, Requena J, Moya JS (1999) J Mater Res 14:3647
13. Ozkan OT, Erkalfa H, Yildirim A (1994) J Eur Ceram Soc 14:351
14. Fang TT, Hwang B, Shiau FS (1989) J Mater Sci Lett 8:1386
15. Ha JS (2000) Ceram Int 26:251
16. ASTM C373–88 (1999) Standard test method for water absorption, bulk density, apparent porosity and apparent specific gravity of fired whiteware products, ASTM International, West Conshohocken, PA

17. Field DP (1997) Ultramicroscopy 67:1
18. Schwarzer RA (1997) Micron 28:249
19. Seabaughs MM, Vaudin MD, Cline JP, Messing GL (2000) J Am Ceram Soc 83:2049
20. Suvaci E, Messing GL (2000) J Am Ceram Soc 83:2041
21. Hillert M (1965) Acta metall 13:227
22. Batti P (1969) Annali Di Chimica 50:1461
23. Goto Y, Takada T (1960) J Am Ceram Soc 43:150
24. Van Hook H (1964) J Am Ceram Soc 47:579
25. Cho SH, Nam HD (1982) Mater Res Bull 17:1265
26. Levin EM (1959) In: Reser MK (ed) Phase diagrams for ceramists. The American Ceramic Society, Columbus, OH
27. Wittenauer MA, Nyenhuis JA, Schlindler AI, Sato H, Friedlaender FJ, Truedson J, Karim R, Patton CE (1993) J Cryst Growth 130:533